Impact Statement

The causal mechanisms of global glaciations are poorly understood. The transition to a Neoproterozoic Snowball Earth after more than 1 Gyr without glaciation represents the most dramatic episode of climate change in the geological record. Here we present new Re-Os geochronology, which, together with existing U-Pb ages, reveal that the glacial period in NW Canada lasted ~55 Myr. Additionally, we present a novel method to track tectonic influences on these climatic perturbations with the first high- resolution coupled Os-Sr isotope curve across the transition from an ice-free world to a Neoproterozoic Snowball Earth. The data indicates that increases in mantle-derived, juvenile material emplaced onto continents and subsequently weathered into the oceans led to enhanced consumption and sequestration of CO_2 into sediments.

Classification: PHYSICAL SCIENCES

Title: Weathering the Snowball

Authors: Alan D. Rooney[1], Francis A. Macdonald[1], Justin V. Strauss[1], Francis Ö. Dudás[2], Christian Hallmann[2,3,4], David Selby[5]

Affiliations: [1] Department of Earth and Planetary Sciences, Harvard University, Cambridge, MA 02138; [2] Department of Earth, Atmospheric and Planetary Sciences, Massachusetts Institute of Technology, Cambridge, MA 02139; [3] Max-Planck-Institute for Biogeochemistry, Hans-Knöll-Strasse 10, 07745 Jena, Germany; [4] MARUM, University of Bremen, Leobener Strasse, 28359 Bremen, Germany; [5] Department of Earth Sciences, Durham University, Durham, DH1 3LE, UK.

Corresponding Author: Alan D. Rooney, Department of Earth and Planetary Sciences, Harvard University, Cambridge, MA 02138, Tel: 617-496-2412, Email: alanrooney@fas.harvard.edu

Keywords: Sturtian, Neoproterozoic, Crygoenian, Snowball Earth, Re-Os geochronology, Strontium isotopes

Abstract.

After nearly a billion years with no evidence for glaciation, ice advanced to equatorial latitudes at least twice between 717 and 635 Ma. Although the initiation mechanism of these Neoproterozoic Snowball Earth events has remained a mystery, the broad synchronicity of rifting of the supercontinent Rodinia, the emplacement of large igneous provinces at low latitude, and the onset of the Sturtian glaciation has suggested a tectonic forcing. We present new Re-Os geochronology and high-resolution Os and Sr isotope profiles bracketing Sturtian-age glacial deposits of the Rapitan Group in NW Canada. Coupled with existing U-Pb dates, the post-glacial Re-Os date of 662.4 ± 3.9 Ma represents the first direct geochronological constraints on both the onset and demise of a Cryogenian glaciation from the same continental margin, and suggest a 55 Myr duration of the Sturtian glacial epoch. The Os and Sr isotope data allow us to assess the relative weathering input of old radiogenic crust and more juvenile, mantle-derived substrate. The pre-glacial isotopic signals are consistent with an enhanced contribution of juvenile material to the oceans and glacial initiation through enhanced global weatherability. In contrast, post-glacial strata feature radiogenic Os and Sr isotope compositions indicative of extensive glacial scouring of the continents and intense silicate weathering in a post-Snowball Earth hothouse.

/body/

The Snowball Earth hypothesis predicts that Neoproterozoic glaciations were global and synchronous at low-latitudes and that deglaciation occurred as a result of the build-up of pCO_2 to extreme levels resulting in a "greenhouse" aftermath (1, 2). The temporal framework of Cryogenian glaciations is built on chemostratigraphy and correlation of lithologically distinct units, such as glaciogenic deposits, iron formation, and cap carbonates (3), tied to the few successions that contain volcanic rocks dated using U-Pb zircon geochronology (4). In strata lacking horizons suitable for U-Pb geochronology, Re-Os geochronology can provide depositional ages on organic-rich sedimentary rocks bracketing glaciogenic strata (5, 6). Moreover, Os isotope stratigraphy can be used as a proxy to test for super-greenhouse weathering during deglaciation (7). In a Snowball Earth scenario we can make specific predictions for Cryogenian weathering: CO_2 consumption via silicate weathering should increase before glaciation, stagnate during the glaciation, and increase again during deglaciation. However, the use of a single weathering proxy to provide evidence for such a scenario, such as Sr isotopes from marine carbonates, is limited both by lithological constraints and an inability to distinguish between the amount of weathering and the composition of what is being weathered (8). The short residence time of Os in the present-day oceans (<10 kyr) (9) provides a complementary higher resolution archive to Sr isotopes and thus, new insights into the nature of extreme fluctuations in the Earth's climate as documented herein.

Stratigraphy of the Neoproterozoic Windermere Supergroup

71 The Neoproterozoic Windermere Supergroup is spectacularly exposed in the Mackenzie
72 Mountains of NW Canada and comprises an ~7 km thick mixed carbonate and siliciclastic
73 marine succession (Fig. 1, Fig. S1). The Coates Lake Group of the Mackenzie Mountains
74 forms the base of the Windermere Supergroup and consists of siliciclastic, carbonate and
75 evaporitic strata of the Thundercloud, Redstone River and Coppercap formations. The
76 Coates Lake Group unconformably overlies the Little Dal Basalt, which has been correlated
77 geochemically with the Tsezotene sills (10), a 777 +2.5/-1.8 Ma ($^{206}Pb/^{238}U$ multi-grain
78 zircon thermal ionization mass spectrometry date) quartz diorite plug near Coates Lake
79 (11), and the ~780 Ma Gunbarrel magmatic event (12).
80 Near Coates Lake, the Coppercap Formation, is ~410 m thick and is separated into 6
81 units (CP1-CP6 in Fig. 2). The Coppercap Formation culminates with a partially
82 dolomitized unit of carbonate conglomerate, with minor sandstone, chert and evaporite
83 (CP6), and is overlain by siltstone and diamictite of the Rapitan Group (Fig. 2).
84 Economic copper deposits grading 3.9% occur in unit CP1 of the Coppercap
85 Formation in a 1 m-thick interval (13, 14). These formed directly below the flooding
86 surface at the base of CP2 (14). Above this, in units CP2-CP5, there is no evidence for
87 mineralization, exposure, or significant sulfate reduction, although minor evaporite and
88 metal showings are present in association with the exposure surfaces at the top of unit CP6.
89 Regionally, the Rapitan Group rests unconformably on the Coates Lake Group, but
90 locally the contact can be gradational (15). In the Ogilvie Mountains, the age of the Rapitan
91 Group is constrained by a $^{206}Pb/^{238}U$ single grain chemical abrasion-isotope dilution-
92 thermal ionization mass spectrometry (CA-ID-TIMS) zircon date of 717.4 ± 0.1 Ma on a
93 rhyolite from the underlying Mount Harper Volcanic Complex, and 716.5 ± 0.2 Ma on a

94 volcanic tuff within the overlying glaciogenic diamictites indicating that glaciation
95 commenced ~717 Ma (4). The Rapitan Group is composed of three formations consisting of
96 stratified and massive glaciogenic diamictites with minor iron formation (16, 17). The
97 lowest unit, the Mount Berg Formation, is present only in the southern Mackenzie
98 Mountains. The overlying Sayunei Formation is locally more than 600 m thick and
99 comprises ferruginous, maroon to dark brown turbiditic siltstone, sandstone, debrites and
100 intervals of stratified and massive glacial diamictite with dropstones of carbonate, basalt
101 and rare granitoid clasts (16, 17). Discontinuous lenticular bodies of hematite-jaspillite iron
102 formation are present near the top of the Sayunei Formation when they are not eroded by
103 the overlying Shezal Formation (17, 18). The uppermost unit of the Rapitan Group, the
104 Shezal Formation, consists of >600 m of green-grey, yellow weathering stratified and
105 massive glacial diamictite interbedded with decameter-scale units of mudstone, siltstone
106 and sandstone, which in some localities unconformably overlies the Sayunei Formation (11,
107 15, 19). Clast composition in the Shezal Formation is highly variable with an abundance of
108 carbonate, altered basic volcanic, sandstone, chert and less common metamorphic pebbles
109 and cobbles (16, 17). An extended duration for deposition of the Rapitan Group is
110 supported by internal unconformities and paleomagnetic poles that shift ~40° from the
111 Mount Berg to Sayunei formations (20).

112 Locally, the basal Twitya Formation of the Hay Creek Group conformably overlies
113 the Rapitan Group, but regionally various parts of the Twitya Formation rest
114 unconformably on underlying strata (19). Where conformable, such as at Mountain River,
115 the basal Twitya Formation consists of a 0-40 m thick ‘cap carbonate’ that is characterized
116 by finely-laminated lime mudstone and siltstone with minor graded beds and sedimentary

117 slump folds (Fig. 2). The lower Twitya Formation is part of a transgressive sequence that
118 passes upwards into fetid, pyritic black shale and then into hundreds of meters of grey-
119 green siltstone and sandstone turbidites. These strata are succeeded by variable siliciclastic
120 and carbonate strata of the Keele Formation and glaciogenic deposits of the Stelfox
121 Member. The Stelfox Member of the Ice Brook Formation consists of massive diamictite
122 with striated clasts (21) and is capped by the Ravensthroat Formation, a white to buff-
123 colored dolostone (17, 22), which hosts sedimentological and geochemical features
124 characteristic of globally distributed ~635 Ma Marinoan cap carbonates (2, 23).
125
126 **Re-Os Geochronology**
127 Organic-lean (<0.5% TOC) cryptalgal laminites of the Coppercap Formation were obtained
128 from drill core and outcrop near Coates Lake (Figs. 1, 2). Core samples were analysed for
129 major and minor elements, carbonate content, C, Sr, and Os isotope chemostratigraphy, and
130 four samples were used for Re-Os geochronology and Os isotope stratigraphy (see SI for
131 details).
132 A Re-Os age of 732.2 ± 3.9 Ma (4.7 Ma including ^{187}Re decay constant uncertainty,
133 n = 4, Mean Square of Weighted Deviates [MSWD] = 1.9, 2σ, initial $^{187}Os/^{188}Os$ = 0.15 ±
134 0.002) was obtained from the Coppercap Formation (Fig. 3a). In conjunction with existing
135 U-Pb zircon ages from the Ogilvie Mountains, this Re-Os age indicates an interval ~15 Myr
136 between deposition of unit CP4 of the Coppercap Formation and Rapitan Group
137 glaciogenic strata (Figs. 1, 2).
138 Organic-rich (>0.5% TOC) micritic limestone of the post-glacial basal Twitya
139 Formation was sampled from outcrop near Mountain River (64°32'04"N, 129°23'42"W).

140 The ‘cap’ limestone was sampled at ~0.5 m resolution for Sr, Os and C isotope
141 chemostratigraphy (24), and a thin (<20 cm) horizon less than 2 m above the Rapitan-
142 Twitya contact was sampled for Re-Os geochronology (Fig. 2). The basal Twitya
143 Formation yielded a Re-Os age of 662.4 ± 3.9 Ma (4.6 Ma including ^{187}Re decay constant
144 uncertainty, n = 7, MSWD = 1.9, 2σ, initial $^{187}Os/^{188}Os$ = 0. 54 ± 0.01; Fig. 3b). The 662.4
145 ± 3.9 Ma Re-Os date for the Twitya Formation together with the CA-ID-TIMS zircon date
146 of 716.5 ± 0.2 Ma from the nearby Ogilvie Mountains (4) represents the first set of age
147 constraints that date both the onset and demise of a Cryogenian glaciation from the same
148 continental margin. Correlation of the Rapitan Group from the Yukon to the Northwest
149 Territories (NWT) is supported not only by the bracketing stratigraphy, but also by the
150 presence of iron formation (25, 26) and paleomagnetic studies that link Rapitan poles from
151 the NWT with the 723–716 Ma Franklin large igneous province (20, 27), which was coeval
152 with Rapitan glaciation in the Yukon (4).
153
154 **Coupled Os and Sr Isotope Stratigraphy**
155 The Os and Sr isotope compositions of seawater have been interpreted to reflect an input
156 balance between radiogenic sources (weathering of upper continental crust and riverine
157 input) and unradiogenic sources (cosmic dust, hydrothermal alteration of oceanic crust and
158 weathering of mafic or ultramafic rocks) (28). However, Os and Sr have distinct sources
159 and sinks, are sensitive to varying geological processes and have contrasting residence
160 times. Therefore, combining these two weathering proxies to investigate Neoproterozoic
161 climatic fluctuations represents a novel method to elucidate the relationship between
162 increased rates of continental weathering and global climate change.

Initial $^{187}Os/^{188}Os$ (Os_i) values from the pre-glacial Coppercap Formation become increasingly unradiogenic up-section from a value of 0.24 to a nadir of 0.12 prior to Rapitan Group deposition (Fig. 2). This extremely low Os_i value is substantially less radiogenic than values reported for modern seawater ($^{187}Os/^{188}Os = 1.06$) (28) and is closer to the primitive upper mantle Os isotope composition (732 Ma = $^{187}Os/^{188}Os = 0.124$) (29). Although it is possible that episodic restriction within the Coates Lake basin, potential hydrothermal input, and/or weathering of a proximal ultramafic body may have contributed to the unradiogenic Os_i values in the Coppercap Formation (Fig. 2), units CP2-CP6 have been previously interpreted to have been deposited in an open marine embayment (14, 30).

In the Coppercap Formation, Sr isotope values are extremely scattered in units CP1-CP3 between 0.7169 and 0.7064, less scattered in units CP4 and CP5 with values converging between 0.7064 and 0.7066, and scattered again in unit CP6. In the Twitya Formation, Sr isotope values decline from 0.7069 to 0.7067 in the basal 5 m and continue to oscillate between 0.7068 and 0.7070 over the ensuing 20 m (Fig. 2; Table S1).

Unlike the Phanerozoic marine Sr isotope curve, whose fidelity can be evaluated by comparisons between several sample types (31), Neoproterozoic marine Sr chemostratigraphy relies exclusively on analyses of whole rock carbonate samples that have potentially been subjected to a variety of diagenetic processes. Based on data from sequential dissolution experiments (32), Sr isotopic analyses of whole rock carbonate samples can be expected to vary in the fourth decimal place, i.e., the external reproducibility of "replicates" from the same sample is ± 0.0001. Sr-isotope measurements are commonly vetted for reliability with Mn/Sr, Sr/Ca, Rb/Sr, and Sr concentration. Mn/Sr is thought to be a sensitive indicator of alteration due to the increase in Mn and decrease of

186 Sr during meteoric alteration (33, 34), however, we find that Mn/Sr and Rb/Sr ratios scale
187 inversely with carbonate content (Table S1). This likely reflects the contamination of small
188 amounts of Sr from clay. Consequently, we cull unreliable results with both low carbonate
189 content and Sr abundance. Above 90% carbonate content and Sr concentrations >650 ppm,
190 $^{87}Sr/^{86}Sr$ scatter above 0.708 is eliminated. However, there is no dependence on carbonate
191 content and Sr concentration, or on Mn/Sr, Rb/Sr, or Sr/Ca on $^{87}Sr/^{86}Sr$ between 0.7064 and
192 0.7080 (Table S1). The lowest and most stratigraphically coherent and reproducible values
193 are in units CP4 and CP5 and in the Twitya Formation. We thus consider these $^{87}Sr/^{86}Sr$
194 measurements as 'most reliable' (Fig. 2; Table S1).
195 The lower Coppercap Formation (units CP1-CP3) contains detrital components
196 derived from the Little Dal Basalt and siliciclastic strata of the Katerine Group (14). These
197 strata have also been geochemically modified by basin-dewatering brines that were
198 responsible for formation of the Coates Lake sediment-hosted Cu deposit. We interpret the
199 radiogenic $^{87}Sr/^{86}Sr$ of the lower Coppercap Formation to reflect effects of both a higher
200 clastic component, and post-depositional modification by basin-dewatering brines.
201
202 **Duration and Synchronicity of the Sturtian Glacial Epoch**
203 The Twitya Formation Re-Os date is identical, within uncertainty, to existing post-glacial
204 U-Pb zircon geochronological data from Australia and South China (Fig. 4) (35, 36),
205 although there are some discrepancies related to analytical procedures of some of the Re-Os
206 ages from Australia (5, 6). Previous work yielded Re-Os age constraints for the Tindelpina
207 Formation (6) which is an amalgamated date based on Re-Os data from two separate drill
208 cores (SCYW-1a and Blinman-2) separated by >100 km. These two horizons were

209 correlated using low-resolution $\delta^{13}C$ stratigraphy, not an accurate technique for sample
210 selection for Re-Os geochronology. The 4-point SCYW1a isochron in their study (6)
211 contains two data points (a3-4 and a3-4r; supplementary data of reference 6 and
212 supplementary Table 5) that are actually two analyses of a single sample suggesting
213 extreme sample heterogeneity. Due to these complications, we consider the SCYW1a age
214 to be misleading and not provide meaningful geochronological data for global correlation.

215 A Re-Os date of 640.7 ± 4.7 Ma from Tasmanian organic-rich rocks has also been
216 used to dispute the synchronicity of the Rapitan-Sturtian deglaciation (5). However, this
217 date from the upper Black River Formation is from a horizon located stratigraphically
218 above two diamictite units that are separated by a carbonate unit, and is overlain by the ca.
219 580 Ma Gaskiers-age Croles Hill diamictite (37). The Croles Hill diamictite was previously
220 correlated with the Marinoan Cottons Breccia on King Island and the Elatina Formation in
221 the Flinders Range of Australia, which implied that the upper Black River Formation was
222 Sturtian in age. However, a new $^{206}Pb/^{238}U$ zircon CA-ID-TIMS date of 636.41 ± 0.45 Ma
223 from the Cottons Breccia (23) suggests that the 640.7 ± 4.7 Ma Re-Os age in the upper
224 Black River Formation is instead correlative with the ca. 635 Ma Marinoan glaciation.

225 The glaciogenic Port Askaig Formation of the Dalradian Supergroup, Scotland was
226 deposited on the NE margin of Laurentia and has been correlated with the Sturtian
227 glaciation using lithostratigraphic and chemostratigraphic techniques (38, 39). A Re-Os age
228 of 659.6 ± 9.6 Ma for the Ballachulish Slate near Loch Leven (40) has been cited as a
229 maximum age constraint for the Port Askaig Formation, however, the Port Askaig is not
230 present in the region, and the relationship of the date to glacigenic strata relies on regional
231 correlations. The broad synchroneity of the Re-Os ages from the Ballachulish Slate

Formation and the Twitya Formation and the apparent disparity in their relationship to glaciogenic horizons calls into question the validity of these ages. A variety of tests on samples from the Ballachulish Slate indicate that the 659.6 ± 9.6 Ma age represents a depositional age and not a mixed age from later metamorphic events (40). Therefore, if we assume that the ages on the Ballachulish and Twitya formations are robust, we are left with the following alternatives: 1) these dates are constraining two separate glaciations during the "Sturtian glacial epoch," and these ages bracket the later event, 2) the Sturtian glaciation is not preserved on the eastern margin of Laurentia and the Port Askaig Formation represents the younger (~635 Ma) Marinoan glaciation and is correlative with the Stralinchy diamictite, or 3) the Kinlochlaggan Boulder Bed is correlative with the Port Askaig Tillite as originally suggested by (41, 42), and as a result, the Ballachulish Slate near Loch Leven would lie in the Argyll Group. Ultimately, additional tests of regional correlations and geochronological constraints are necessary to more fully resolve the complexities of the Dalradian Supergroup.

Existing $^{206}Pb/^{238}U$ zircon ages from Idaho have been previously used to argue that the Sturtian glaciation is globally diachronous (43, 44). However, these ages, coupled with the 711.5 ± 0.3 Ma age from the Gubrah Formation in Oman (45), can also be interpreted to be syn-glacial constraints and correlative with the 717–662 Ma Sturtian glacial epoch recorded in NW Canada (Fig. 4). Additional constraints from U-Pb and Re-Os geochronology are necessary to determine if Sturtian glacial strata represent a series of glacial-interglacial cycles (46), a Jormagund climate state (47), or a continuous ~55 Myr Snowball Earth event.

It has also been suggested that there was an earlier, ca. 750 Ma glaciation recorded on the Kalahari (48), Congo (49), and Tarim (50) cratons. However, there is no direct evidence for glaciation in Kaigas Formation on the Kalahari Craton (51), and the ages from the Congo and Tarim cratons suffer from inheritance and cannot be relied on (see concordia diagrams in references 49 and 50). Our Re-Os age of 732.2 ± 3.9 Ma on the Coppercap Formation coupled with global C and Sr isotope correlation is further consistent with the lack of evidence for a pre-717 Ma glaciation. The large negative carbon isotope anomaly in the lower Coppercap Formation covaries in carbonate carbon and organic carbon isotopes (Fig. 2) and can be correlated with the Islay anomaly in Scotland, Greenland, and Svalbard (3), consistent with pre-Sturtian Sr isotope values (52, 53). However, the Islay anomaly in Scotland is not present in the Loch Leven region in Scotland and its relationship to the dated Ballachulish Slate (40) is unclear. The Re-Os geochronology presented here suggests that the Islay anomaly returns to positive $\delta^{13}C_{carb}$ values by ~732 Ma, well before the onset of glaciation at ~717 Ma (4) and thus cannot be mechanistically linked to the onset of glaciation as has been previously proposed (54-56). Moreover, none of these successions host any evidence for glaciation prior to the Islay anomaly.

Fire and Ice Revisited

The Sr isotope data reported here at ca. 732 Ma – as low as ~0.7064 in the Coppercap Formation – are consistent with other low pre-Sturtian values recorded in strata from Svalbard and Greenland (52, 53) and are less radiogenic then the ca. 780 Ma values from Svalbard (57). Interestingly, Nd isotope studies have also suggested an increase to more mantle-like (more radiogenic) values tens of millions of years prior to the Sturtian

277 glaciation (57). These data are consistent with the 'Fire and Ice' hypothesis (58, 59), which
278 proposes that Cryogenian glaciations were initiated through enhanced CO_2 consumption via
279 weathering of basalts emplaced at low-latitudes. The low-latitude breakup of Rodinia is
280 thought to have been associated with the development of multiple juvenile volcanic rift
281 margins and the emplacement of multiple large igneous provinces (e.g., Willouran, Guibei,
282 Gunbarrel, and Franklin LIPs) (60). Enhanced volcanism and weathering of mafic material
283 would have driven the ocean towards more unradiogenic Sr values and mantle-like Os_i
284 values and a cooler global climate (Fig. 4), analogous to scenarios proposed for Mesozoic
285 ocean anoxic events and Cenozoic cooling episodes (61-63).

286 In sharp contrast, the Os_i data from the overlying Twitya Formation yield a
287 radiogenic signal for the post-glacial ocean with the basal cap limestone recording an Os_i
288 value of 1.44. From this initial high, values decline rapidly reaching a nadir of 0.42 at a
289 height 2.6 m above the diamictite, then become steadily more radiogenic to a value of 0.62
290 before stabilizing to values ~0.50 above 10 m (Fig. 2). Similarly, Sr isotope values decrease
291 from 0.7068 to 0.7066 in the lower 3 m and continue to fluctuate up section to before
292 levelling out between 0.7068 and 0.7070. We interpret the signal recorded in the lower 3 m
293 to represent the highly radiogenic, unmixed glacial melt water plume (64) and a subsequent
294 decrease to less radiogenic Sr isotope values at 3–10 m to reflect the transgression of
295 glacial deep waters (65). Up-section, it appears as though rapid mixing obscures the melt
296 water signal; however, enhanced silicate weathering continued through the transgression in
297 a high pCO_2 environment, resulting in an Os_i much more radiogenic than pre-glacial values
298 that complement the radiogenic trend recorded in the coeval Sr composition of seawater
299 (Fig. 2). The absence of a trend to unradiogenic Sr isotope values across Cryogenian glacial

deposits led some workers to conclude that Neoproterozoic glaciations were short-lived (<1 Myr) (66). However, this approach neglects carbonate dissolution in response to ocean acidification and assumes that the Sr cycle is in steady state (67, 68), which is inconsistent with the sharp rise seen in globally distributed cap carbonate deposits.

Sr isotope data from Sturtian cap limestones in Namibia, Mongolia, and NW Canada agree to the fourth decimal place (69,70) thereby supporting a global correlation of this trend (Fig. 5). These Sr values increase rapidly from 0.7066 to 0.7072 in the Sturtian cap carbonate sequence and then flat-line through the rest of the Cryogenian period. Thus, the Neoproterozoic rise in seawater Sr isotope values may not have been gradual, as previously suggested (52), but stepwise and driven by extreme weathering in a post-glacial super-greenhouse.

Conclusions

The geological record suggests that the Earth's climate system can exist in two climatic equilibria, one globally glaciated and the other not (46, 47). However, both the processes that maintain a steady climate and the drivers of long-term (>10 Myr) climate change have remained obscure. Following a billion years of relative climatic stability with no apparent glacial deposits, the Neoproterozoic witnessed the transition from an ice-free world to a Snowball Earth. The new Os and Sr isotope stratigraphy coupled with the Re-Os geochronology data presented herein also point towards a tectonic driver for long-term climate change and that the change in global weatherability may have been driven by a relative increase in juvenile, mantle-derived material weathered into the oceans from the continents.

Initiation of a Snowball Earth through a change in global weatherability has been criticized on the grounds that these background conditions should have persisted on >10 Myr timescale and after deglaciation the Earth should have rapidly returned to a Snowball state (46). Our new constraint of a ~55 Myr duration of the Sturtian glacial epoch in NW Canada is consistent with a short interlude between the Sturtian and Marinoan glaciations and a return to a glacial state on a timescale consistent with enhanced weatherability (71). Enhanced input of mantle-derived material to the ocean would have also influenced geochemical cycles and promoted anaerobic respiration, potentially providing additional feedbacks that conspired to initiate a Neoproterozoic Snowball Earth (54). Our results confirm that the Sturtian glacial epoch was long lasting, its onset was accompanied by basalt-dominated weathering, and its termination was globally synchronous and followed by extreme weathering of the continents. The post-Sturtian weathering event may have in turn provided limiting nutrients like phosphorous to the ocean (72), leading to an increase in atmospheric oxygen and the radiation of large animals with high metabolic demands.

ACKNOWLEDGMENTS. We thank Rigel Lustwerk for providing samples from the 6YR core. We are grateful to the Yukon Geological Survey, Roger Summons and MIT's NAI astrobiology node for support. We thank Roger Summons, Sam Bowring and Dan Schrag for the use of their labs. The Durham Laboratory for Source Rock Geochronology and Geochemistry is partially funded by TOTAL and BP. CH was supported by the Agouron Institute. We wish to acknowledge the superb teams at Canadian and Fireweed helicopter companies and Dugald Dunlop from Meridian Mining via Colorado Minerals. We thank three reviewers and Paul Hoffman for comments on the manuscript and editorial advice.

1. Hoffman PF, Kaufman AJ, Halverson GP, & Schrag DP (1998) A Neoproterozoic Snowball Earth. *Science* 281:1342-1346.

2. Hoffman PF & Schrag DP (2002) The snowball Earth hypothesis; testing the limits of global change. *Terra Nova* 14(3):129-155.
3. Halverson GP, Hoffman PF, Schrag DP, Maloof AC, & Rice AHN (2005) Toward a Neoproterozoic composite carbon-isotope record. *Geological Society of America Bulletin* 117(9-10):1181-1207.
4. Macdonald FA*, et al.* (2010) Calibrating the Cryogenian. *Science* 327:1241-1243.
5. Kendall BS, Creaser RA, Calver CR, Raub TD, & Evans DAD (2009) Correlation of Sturtian diamictite successions in southern Australian and northwestern Tasmania by Re-Os black shale geochronology and the ambiguity of "Sturtian"-type diamictite-cap carbonate pairs as chronostratigraphic marker horizons. *Precambrian Research* 172:301-310.
6. Kendall BS, Creaser RA, & Selby D (2006) Re-Os geochronology of postglacial black shales in Australia: constraints on the timing of "Sturtian" glaciation. *Geology* 34:729-732.
7. Ravizza G & Peucker-Ehrenbrink B (2003) The marine $^{187}Os/^{188}Os$ record of the Eocene-Oligocene transition: the interplay of weathering and glaciation. *Earth and Planetary Science Letters* 210:151-165.
8. Raymo ME & Ruddiman WF (1992) Tectonic forcing of late Cenozoic climate. *Nature* 359:117-122.
9. Paquay FS & Ravizza G (2012) Heterogeneous seawater $^{187}Os/^{188}Os$ during the Late Pleistocene glaciations. *Earth and Planetary Science Letters* 349:126-138.
10. Dudás FO & Lustwerk RL (1997) Geochemistry of the Little Dal basalts: continental tholeiites from the Mackenzie Mountains, Northwest Territories, Canada. *Canadian Journal of Earth Sciences* 34:50-58.
11. Jefferson CW & Parrish R (1989) Late Proterozoic stratigraphy, U/Pb zircon ages and rift tectonics, Mackenzie Mountains, northwestern Canada. *Canadian Journal of Earth Sciences* 26:1784-1801.
12. Harlan SS, Heaman LM, LeCheminant AN, & Premo WR (2003) Gunbarrel mafic magmatic event: a key 780 Ma time marker for Rodinia plate reconstructions. *Geology* 31:1053-1056.
13. Chartrand FM & Brown AC (1985) The diagenetic origin of stratiform copper mineralization, Coates Lake, Redstone Copper belt, NWT, Canada. *Economic Geology* 80:325-343.
14. Lustwerk RL (1990) Geology and geochemistry of the Redstone strataform copper deposit, Northwest Territories, Canada. PhD (Pennsylvania State University).
15. Helmstaedt H, Eisbacher GH, & McGregor JA (1979) Copper mineralization near an intra-Rapitan unconformity, Nite copper prospect, Mackenzie Mountains, Northwest Territories, Canada. *Canadian Journal of Earth Sciences* 16:50-59.
16. Eisbacher GH (1978) Redefinition and subdivision of the Rapitan Group, Mackenzie Mountains. *Geological Survey of Canada Paper 77-35*:1-21.
17. Hoffman PF & Halverson GP (2011) Neoproterozoic glacial record in the Mackenzie Mountains, northern Canadian Cordillera. *The Geological Record of Neoproterozoic Glaciations*, eds Arnaud E, Halverson GP, & Shields-Zhou G (The Geological Society, London), Vol 36, pp 397-412.

18. Klein C & Beukes NJ (1993) Sedimentology and geochemistry of the glaciogenic late Proterozoic Rapitan iron-formation in Canada. *Economic Geology* 84:1733-1774.
19. Eisbacher GH (Sedimentary tectonics and glacial record in the Windermere Supergroup, Mackenzie Mountains, northwestern Canada. Geological Survey of Canada Paper 80-27, pp 1-40.
20. Park JK (1997) Paleomagnetic evidence for low-latitude glaciation during deposition of the Neoproterozoic Rapitan Group, Mackenzie Mountains, N.W.T., Canada. *Canadian Journal of Earth Sciences* 34:34-49.
21. Aitken JD (1991) The Ice Brook Formation and Post-Rapitan, Late Proterozoic glaciation, Mackenzie Mountains, Northwest Territories. *Geological Survey of Canada Bulletin* 404:1-43.
22. James NP, Narbonne GM, & Kyser TK (2001) Late Neoproterozoic cap carbonates: Mackenzie Mountains, northwestern Canada: precipitation and global glacial meltdown. *Canadian Journal of Earth Sciences* 38(8):1229-1262.
23. Calver CR*, et al.* (2013) Globally synchronous Marinoan deglaciation indicated by U-Pb geochronology of the Cottons Breccia, Tasmania, Australia. *Geology* 41:1127-1130.
24. Johnston DT, Macdonald FA, Gill B, Hoffman PF, & Schrag DP (2012) Uncovering the Neoproterozoic carbon cycle. *Nature* 483(7389):320-323.
25. Young GM (1976) Iron-formation and glaciogenic rocks of the Rapitan Group, Northwest Territories, Canada. *Precambrian Research* 3:137-158.
26. Young GM (1982) The late Proterozoic Tindir Group, east-central Alaska; Evolution of a continental margin. *Geological Society of America Bulletin* 93:759-783.
27. Denyszyn SW, Halls HC, Davis DW, & Evans DAD (2009) Paleomagnetism and U-Pb geochronology of Franklin dykes in High Arctic Canada and Greenland: a revised age and paleomagnetic pole for constraining block rotations in the Nares Strait region. *Canadian Journal of Earth Sciences* 46:689-705.
28. Peucker-Ehrenbrink B & Ravizza G (2000) The marine osmium isotope record. *Terra Nova* 12:205-219.
29. Meisel T, Walker RJ, Irving AJ, & Lorand J-P (2001) Osmium isotopic compositions of mantle xenoliths: a global perspective. *Geochimica et Cosmochimica Acta* 65:1311-1323.
30. Jefferson CW (1978) The Upper Proterozoic Redstone Copper Belt, Mackenzie Mountains, Northwest Territories. Ph.D (University of Western Ontario, London).
31. Brand U (2004) Carbon, oxygen and strontium isotopes in Paleozoic carbonate components: an evaluation of original seawater-chemistry proxies. *Chemical Geology* 204:23-44.
32. Li D, Shields-Zhou G, Ling HF, & Thirwall M (2011) Dissolution methods for strontium isotope stratigraphy: Guidelines for the use of bulk carbonate and phosphorite rocks. *Chemical Geology* 290:133-144.
33. Derry LA, Keto LS, Jacobsen SB, Knoll AH, & Swett K (1989) Sr isotopic variations in Upper Proterozoic carbonates from Svalbard and East Greenland. *Geochmica et Cosmochimica Acta* 53(9):2231-2339.

34. Banner JL & Hanson GN (1990) Calculation of simultaneous isotopic and trace element variations during water-rock interaction with application to carbonate diagenesis. *Geochimica et Cosmochimica Acta* 54:3123-3137.
35. Fanning CM & Link PK (2008) Age constraints for the Sturtian glaciation: data from the Adelaide Geosyncline, South Australia and Pocatello Formation Idaho, USA. *Geological Society of Australia Abstracts, No. 91, Selwyn Symposium 2008, Melbourne*:57-62.
36. Zhou C*, et al.* (2004) New constraints on the ages of Neoproterozoic glaciations in south China. *Geology* 32:437-440.
37. Calver CR, Black LP, Everard JL, & Seymour DB (2004) U-Pb zircon age constraints on late Neoproterozoic glaciation in Tasmania. *Geology* 32(10):893-896.
38. Brasier MD & Shields G (2000) Neoproterozoic chemostratigraphy and correlation of the Port Askaig glaciation, Dalradian Supergroup of Scotland. *Journal of the Geological Society of London* 157:909-914.
39. Prave AR, Fallick AE, Thomas CW, & Graham CM (2009) A composite C-isotope profile for the Neoproterozoic Dalradian Supergroup of Scotland and Ireland. *Journal of the Geological Society of London* 166:1-13.
40. Rooney AD, Chew DM, & Selby D (2011) Re-Os geochronology of the Neoproterozoic-Cambrian Dalradian Supergroup of Scotland and Ireland: implications for Neoproterozoic stratigraphy, glaciation and Re-Os systematics. *Precambrian Research* 185:202-214.
41. Treagus JE (1969) The Lower Dalradian Kinlochlaggan Boulder Bed, central Scotland. *Earth pre-Pleistocene glacial record*, eds Hambrey MJ & Harland WB (Cambridge University Press, Cambridge, UK), pp 637-639.
42. Evans RHS & Tanner PWG (1996) A late Vendian age for the Kinlochlaggan Boulder Bed (Dalradian)? *Journal of the Geological Society, London* 153:823-826.
43. Fanning CM & Link PK (2004) U-Pb SHRIMP ages of Neoproterozoic (Sturtian) glaciogenic Pocatello Formation, southeastern Idaho. *Geology* 32:881-884.
44. Keeley JA, Link PK, Fanning CM, & Schmitz MD (2013) Pre- to synglacial rift-related volcanism in the Neoproterozoic (Cryogenian) Pocatello Formation, SE Idaho: New SHRIMP and CA-ID-TIMS constraints. *Lithosphere* 5(1):128-150.
45. Bowring SA, Grotzinger JP, Condon DJ, Ramezani J, & Newall M (2007) Geochronologic constraints on the chronostratigraphic framework of the Neoproterozoic Huqf Supergroup, Sultanate of Oman. *American Journal of Science* 307:1097-1145.
46. Pierrehumbert RT, Abbot DS, Voigt A, & Koll D (2011) Climate of the Neoproterozoic. *Annual Review of Earth and Planetary Sciences* 39:417-460.
47. Abbot DS, Voigt A, & Koll D (2011) The Jormungand global climate state and implications for Neoproterozoic glaciations. *Journal of Geophysical Research* 116(D18103).
48. Frimmel HE, Klotzli US, & Siegfried PR (1996) New Pb-Pb single zircon age constraints on the timing of Neoproterozoic glaciation and continental break-up in Namibia. *Journal of Geology* 104:459-469.
49. Key RM*, et al.* (2001) The western arm of the Lufilian Arc in NW Zambia and its potential for copper mineralization. *Journal of African Earth Sciences* 33:503-528.

50. Xu B, *et al.* (2009) SHRIMP zircon U-Pb age constraints on Neoproterozoic Quruqtagh diamictites in NW China. *Precambrian Research* 168:247-258.
51. Macdonald FA, Strauss JV, Rose CV, Dudás FO, & Schrag DP (2010) Stratigraphy of the Port Nolloth Group of Namibia and South Africa and implications for the age of Neoproterozoic iron formations. *American Journal of Science* 310:862-888.
52. Halverson GP, Dudás FO, Maloof AC, & Bowring SA (2007) Evolution of the $^{87}Sr/^{86}Sr$ composition of Neoproterozoic seawater. *Palaeogeography Palaeoclimatology Palaeoecology* 256:103-129.
53. Fairchild IJ, Spiro B, Herrington PM, & Song T (2000) Controls on Sr and C isotope compositions of Neoproterozoic Sr-rich limestones of East Greenland and North China. *Carbonate Sedimentation and Diagenesis in the Evolving Precambrian World*, eds Grotzinger JP & James NP (SEPM Special Publication, Tulsa), Vol 67, pp 297-313.
54. Tziperman E, Halevy I, Johnston DT, Knoll AH, & Schrag DP (2011) Biologically induced initiation of Neoproterozoic snowball-Earth events. *Proceedings of the National Academy of Sciences* 108(108):15091-15096.
55. Hoffman PF*, et al.* (2012) Cryogenian glaciations on the southern tropical paleomargin of Laurentia (NE Svalbard and East Greenland), and a primary origin for the upper Russoya (Islay) carbon isotope excursion. *Precambrian Research* 206-207:137-158.
56. Schrag DP, Berner RA, Hoffman PF, & Halverson GP (2002) On the initiation of snowball Earth. *Geochemistry, Geophysics, Geosystems* 3.
57. Halverson GP, Wade BP, Hurtgen MT, & Barovich KM (2010) Neoproterozoic Chemostratigraphy. *Precambrian Research* 182(4):337-350.
58. Donnadieu Y, Godderis Y, Ramstein G, Nedelec A, & Meert J (2004) A 'snowball Earth' climate triggered by continental break-up through changes in runoff. *Nature* 428:303-306.
59. Godderis Y*, et al.* (2003) The Sturtian 'snowball' glaciation: fire and ice. *Earth and Planetary Science Letters* 6648:1-12.
60. Li ZX*, et al.* (2008) Assembly, configuration, and break-up history of Rodinia: A synthesis. *Precambrian Research* 160(1-2):179-210.
61. Ravizza G & Peucker-Ehrenbrink B (2003) Chemostratigraphic evidence of Deccan volcanism from the marine osmium isotope record. *Science* 302:1392-1395.
62. Turgeon SC & Creaser RA (2008) Cretaceous oceanic anoxia event 2 triggered by a massive magmatic episode. *Nature* 454:323-327.
63. Kent DV & Muttoni G (2013) Modulation of Late Cretaceous and Cenozoic climate by variable drawdown of atmospheric pCO_2 from weathering of basaltic provinces on continents drifting through the equatorial humid belt. *Climates of the Past.* 9: 525-546.
64. Shields G (2005) Neoproterozoic cap carbonates: a critical appraisal of existing models and the plumeworld hypothesis. *Terra Nova* 17(4):299-310.
65. Hoffman PF*, et al.* (2007) Are basal Ediacaran (635 Ma) post-glacial "cap dolostones" diachronous? *Earth and Planetary Science Letters* 258:114-131.
66. Jacobsen S & Kaufman AJ (1999) The Sr, C, and O isotopic evolution of Neoproterozoic seawater. *Chemical Geology* 161:37-57.

67. Le Hir G, Ramstein G, Donnadieu Y, & Godderis Y (2008) Scenario for the evolution of atmospheric pCO2 during a snowball Earth. *Geology* 36:47-50.
68. Higgins JA & Schrag DP (2003) Aftermath of a snowball Earth. *Geophysics, Geochemistry, Geosystems* 4:1-20.
69. Yoshioka H, Asahara Y, Tojo B, & Kawakami S (2003) Systematic variations in C and Sr isotopes and elemental concentrations in Neoproterozoic carbonates in Namibia: implications for a glacial to interglacial transition. *Precambrian Research* 124:69-85.
70. Shields G, Brasier MD, Stille P, & Dorjnamjaa D (2002) Factors contributing to high $\delta^{13}C$ values in Cryogenian limestones of western Mongolia. *Earth and Planetary Science Letters* 196:99-111.
71. Mills B, Watson AJ, Goldblatt C, Boyle RA, & Lenton TM (2011) Timing of Neoproterozoic glaciations linked to transport-limited global weathering. *Nature Geoscience* 4:861-864.
72. Planavsky NJ*, et al.* (2010) The evolution of the marine phosphate reservoir. *Nature* 467:1088-1090.

Figure Legends.

Fig. 1. Schematic stratigraphy of Tonian, Cryogenian and Ediacaran strata of the Mackenzie and Ogilvie Mountains. U-Pb ages are from ref. (4) and Re-Os ages are from this work (Reefal Ass, Reefal Assemblage; Mt, Mount; V.C., volcanic complex; Congl., conglomerate; Coates Lk, Coates Lake; Thund., Thundercloud Formation; Cu-cap, Coppercap Formation).

Fig. 2. Composite chemo- and lithostratigraphy of the Windermere Supergroup from the Mackenzie Mountains, Canada (measured sections F1173, P5C and 6YR). Organic carbon isotope data for the Twitya Formation in Section P5C is from (24) (Say, Sayunei; Sh, Shezal). The superscript next to 716 and 717 Ma corresponds to the cited reference.

Fig. 3. (*A*) Re-Os isochron for the Coppercap Formation with an age uncertainty of 4.7 Ma when the uncertainty in the ^{187}Re decay constant is included. (*B*) Re-Os isochron for the Twitya Formation with an age uncertainty of 4.6 Ma when the uncertainty in the ^{187}Re decay constant is included. Isotope composition and abundance data are presented in Table S2.

Fig. 4. (*A*) Compilation of initial ^{187}Os/^{188}Os isotope data and ^{87}Sr/^{86}Sr data for pre- and post-Sturtian successions worldwide (5, 6, 40, 53, 70). All data are in Tables S1-5. (*B*) Geological cartoon of Neoproterozoic pre-glacial weathering fluxes. (*C*) Geological cartoon of post-glacial weathering fluxes. See text and SI for further details.

Supplementary Table 1: TOC, carbon, strontium, oxygen isotope and trace element data for sections of Coppercap and Twitya formations.

Rapitan	Sample	Height in m (from base of CC)	Lithology	TOC (wt %)	δ^{13}Ccarb ‰ (VPDB)	δ^{18}O ‰ (VPDB)	$^{87}Sr/^{86}Sr$	δ^{13}C org ‰ (VPDB)	C Epsilon ‰	Sr (ppm)	Mn (ppm)	Mn/Sr	% CARB	Rb/Sr	Mg/Ca
6YR	76	421.2	gy gs wacke	0.02	2.70	-10.95	0.71021	-36.39	39.09	-	-	-	-	-	-
6YR	77	416.7	diamictite	-	3.68	-10.35	0.71050	-	-	704	4486	6.372	24.7	0.0240	0.07866
6YR	78	416.6	gy microbial	-	4.43	-10.79	0.70987	-	-	344	1404	4.080	81.4	0.0101	0.06254
6YR	79	413.7	gy gs	0.01	3.65	-8.64	0.70981	-37.02	40.67	366	1232	3.365	54.3	0.0052	0.18743
6YR	80	408.2	gy micrite	0.01	5.70	-11.45	0.70841	-25.72	31.42	295	102	0.345	100.1	0.0021	0.00726
6YR	81	405.2	wht brecc dol	-	6.10	-15.15	0.70762	-	-	204	152	0.746	81.5	0.0023	0.00338
6YR	82	402.4	wht brecc dol	-	6.08	-15.88	0.70714	-	-	-	-	-	-	-	-
6YR	83	396.7	wht brecc dol	-	-7.30	-6.41	0.70662	-	-	-	-	-	-	-	-
6YR	84	393.5	dgy gs wacke	0.03	3.69	-4.37	0.70665	-22.83	26.53	1428	83	0.058	82.5	0.0006	0.18079
6YR	85	379.9	dgy micrite	0.04	6.28	-2.60	0.70667	-20.96	27.24	1583	50	0.032	76.9	0.0003	0.60862
6YR	86	376.0	dgy micrite	-	5.35	-4.13	0.70668	-	-	1957	74	0.038	80.5	0.0003	0.19336
6YR	87	374.7	gy gs	0.01	6.72	-4.43	0.70667	-26.89	33.61	-	-	-	-	-	-
6YR	88	368.9	gy gs	-	6.46	-5.26	0.70665	-	-	1866	95	0.051	68.4	0.0002	0.18952
6YR	89	363.4	gy gs, ev	0.07	5.76	-4.90	0.70657	-31.03	36.79	-	-	-	-	-	-
6YR	90	358.2	dgy micrite	-	5.72	-5.12	0.70664	-	-	1489	374	0.251	95.6	0.0003	0.03695
6YR	91	353.1	dgy micrite	0.04	7.04	-7.05	0.70653	-18.04	25.09	695	40	0.058	101.1	0.0005	0.00788
6YR	92	347.2	dgy micrite	0.09	5.30	-5.45	0.70667	-22.38	27.67	902	173	0.192	98.0	0.0007	0.05230
6YR	93	341.8	dgy micrite	-	5.08	-5.63	0.70666	-	-	973	118	0.121	98.3	0.0011	0.09666
6YR	94	337.2	dgy micrite	-	6.53	-3.93	0.70651	-	-	807	51	0.063	99.9	0.0005	0.00909
6YR	95	331.2	dgy micrite	0.08	6.59	-3.66	0.70649	-20.53	27.12	1117	51	0.046	93.9	0.0003	0.00895
6YR	96	325.5	dgy microbial	-	6.33	-3.52	0.70650	-	-	1267	74	0.058	98.1	0.0009	0.01123
6YR	97	321.2	dgy micrite	0.08	6.15	-4.33	0.70648	-20.55	26.70	1016	70	0.068	98.8	0.0004	0.01024
6YR	98	315.2	dgy gs wacke	-	4.95	-4.13	0.70650	-	-	1355	109	0.080	98.3	0.0006	0.01337
6YR	99	311.7	dgy micrite	0.06	4.72	-4.44	0.70648	-22.54	27.26	982	59	0.060	99.9	0.0004	0.01807
6YR	100	305.2	dgy gs	0.05	3.30	-5.30	0.70659	-25.65	28.95	1205	67	0.056	98.7	0.0003	0.02124
6YR	101	299.2	gy gs	0.11	4.42	-4.27	0.70660	-25.88	30.30	2048	99	0.048	86.9	0.0012	0.04859
6YR	102	292.0	dgy micrite	0.23	2.64	-3.53	0.70668	-24.16	26.80	1148	709	0.618	50.2	0.0081	0.41265
6YR	103	284.2	dgy gs	-	2.48	-3.74	0.70674	-	-	1166	157	0.134	50.7	0.0023	0.12620
6YR	104	277.2	dgy micrite	0.23	2.98	-4.04	0.70669	-25.82	28.80	828	144	0.175	89.8	0.0035	0.14382

6YR	105	268.7	dgy micrite	0.48	2.00	-3.98	0.70691	-26.92	28.92	1189	103	0.086	89.7	0.0017	0.05358
6YR	106	262.6	dgy micrite	0.36	0.41	-2.79	0.70713	-25.67	26.08	772	347	0.449	83.3	0.0056	0.53384
6YR	107	255.2	dgy micrite	-	0.71	-4.36	0.70704	-	-	1187	104	0.088	59.1	0.0022	0.10019
6YR	108	249.9	gy gs	0.08	0.71	-6.76	0.70706	-29.31	30.02	1142	25	0.022	84.3	0.0012	0.05783
6YR	109	242.8	gy gs	-	-1.53	-5.30	0.70683	-	-	1699	115	0.068	94.3	0.0005	0.55264
6YR	110	235.7	gy gs	0.03	0.29	-3.77	0.70691	-28.75	29.04	1446	96	0.067	60.1	0.0005	0.58983
6YR	111	229.8	dgy gs	-	0.09	-4.73	0.70751	-	-	684	68	0.099	50.2	0.0011	0.11193
6YR	112	222.5	gy microbial	0.57	-0.86	-5.94	0.70781	-30.06	29.20	-	-	-	-	-	-
6YR	113	217.0	gy gs	0.30	-2.37	-2.90	0.71107	-31.16	28.79	251	720	2.872	95.1	0.0574	0.67578
6YR	114	208.5	dgy micrite	0.45	-3.39	-6.92	0.70939	-33.38	29.99	-	-	-	-	-	-
6YR	115	201.8	dgy microbial	0.08	-2.19	-4.85	0.71457	-28.87	26.67	-	-	-	-	-	-
6YR	116	194.8	dgy micrite	-	-4.54	-3.77	0.70969	-	-	287	1184	4.119	42.3	0.0310	0.66623
6YR	117	188.2	dgy micrite	1.39	-4.29	-5.58	0.70644	-31.88	27.59	327	824	2.523	51.5	0.0313	0.32804
6YR	118	180.7	dgy micrite	0.17	-5.32	-7.07	0.71280	-30.94	25.62	714	709	0.992	15.1	0.0043	0.06225
6YR	119	173.2	dgy micrite	-	-3.28	-4.66	0.71352	-	-	-	-	-	-	-	-
6YR	120	168.1	dgy wacke	0.11	-5.02	-6.20	0.70787	-32.34	27.32	888	1110	1.249	57.2	0.0015	0.21395
6YR	122	152.5	dgy micrite	-	-4.87	-4.90	0.71289	-	-	198	1788	9.037	61.1	0.0462	0.77903
6YR	123	145.1	dgy micrite	0.17	-4.94	-5.58	0.71324	-31.80	26.86	-	-	-	-	-	-
6YR	125	97.5	gy micrite	0.11	-6.09	-6.17	0.71266	-32.05	25.96	341	1514	4.441		0.0810	0.31223
6YR	128	99.4	gy micrite	0.26	-4.42	-4.70	0.71688	-31.97	27.55	157	1652	10.508	37.3	0.0741	0.60216
6YR	129	124.1	gy micrite	0.09	-3.65	-5.01	0.71550	-31.48	27.83	636	179	0.281	79.3	0.0038	0.08526
6YR	130	131.2	gy micrite	0.11	-5.10	-4.74	0.71178	-31.49	26.39	-	-	-	27.2	-	-

Twitya	**Sample**	**Height in m (from contact with Shezal)**	**Lithology**	**TOC (wt %)**	**δ^{13}Ccarb ‰ (VPDB)**	**δ^{18}O ‰ (VPDB)**	**$^{87}Sr/^{86}Sr$**	**δ^{13}C org ‰ (VPDB)**	**C Epsilon ‰**	**Sr (ppm)**	**Mn (ppm)**	**Mn/Sr**	**% CARB**	**Rb/Sr**	**Mg/Ca**
F1173	0.1	0.1	dgy lime micrite	-	-2.10	-8.40	0.70693	-	-	641	468	0.701	96.1	-	0.01235
F1173	0.5	0.5	dgy lime micrite	-	-2.69	-8.66	0.70751	-	-	-	-	-	-	-	-
F1173	1.0	1.0	dgy lime micrite	-	-2.47	-8.56	0.70690	-	-	-	-	-	-	-	-
F1173	1.6	1.6	dgy lime micrite	-	-0.95	-8.89	0.70686	-	-	-	-	-	-	-	-
F1173	2.0	2.0	dgy lime micrite	-	-1.50	-6.92	0.70678	-	-	-	-	-	-	-	-
F1173	2.6	2.6	dgy lime micrite	-	-0.94	-8.53	0.70681	-	-	-	-	-	-	-	-
F1173	3.1	3.1	dgy lime micrite	-	-0.66	-8.41	0.70672	-	-	2763	176	0.062	98.0	-	0.01235

F1173	3.0	3.0	dgy lime micrite	-	-0.89	-8.73	-	-	-	-	-	-	-	-	-
F1173	3.7	3.7	dgy lime micrite	-	-	-	0.70675	-	-	-	-	-	-	-	-
F1173	4.3	4.3	dgy lime micrite	-	-0.74	-8.77	-	-	-	-	-	-	-	-	-
F1173	4.9	4.9	dgy lime micrite	-	-0.65	-8.80	0.70682	-	-	-	-	-	-	-	-
F1173	5.5	5.5	dgy lime micrite	-	-0.50	-8.78	0.70681	-	-	-	-	-	-	-	-
F1173	6.0	6.0	dgy lime micrite	-	-0.78	-9.03	0.70680	-	-	2825	439	0.149	96.0	-	0.03005
F1173	6.5	6.5	dgy lime micrite	-	-0.59	-8.83	-	-	-	-	-	-	-	-	-
F1173	7.0	7.0	dgy lime micrite	-	-0.67	-8.90	-	-	-	-	-	-	-	-	-
F1173	7.5	7.5	dgy lime micrite	-	-0.92	-8.60	0.70676	-	-	3345	209	0.061	98.0	-	0.01344
F1173	8.0	8.0	dgy lime micrite	-	-0.90	-9.25	0.70676	-	-	3052	210	0.069	100.0	-	0.01487
F1173	8.5	8.5	dgy lime micrite	-	-0.90	-9.03	-	-	-	-	-	-	-	-	-
F1173	9.0	9.0	dgy lime micrite	-	-0.93	-9.08	-	-	-	-	-	-	-	-	-
F1173	9.5	9.5	dgy lime micrite	-	-0.98	-9.07	0.70674	-	-	3808	137	0.035	98.0	-	0.01118
F1173	10.0	10.0	dgy lime micrite	-	-0.87	-9.26	-	-	-	-	-	-	-	-	-
F1173	10.5	10.5	dgy lime micrite	-	-0.51	-9.25	0.70682	-	-	2248	761	0.332	98.0	-	0.03263
F1173	11.0	11.0	dgy lime micrite	-	-0.34	-8.80	0.70685	-	-	2082	468	0.225	100.0	-	0.02748
F1173	11.5	11.5	dgy lime micrite	-	-0.25	-8.82	0.70677	-	-	3007	597	0.198	100.0	-	0.03911
F1173	12.0	12.0	dgy lime micrite	-	-0.55	-8.81	0.70681	-	-	2761	579	0.210	100.0	-	0.11319
F1173	12.5	12.5	dgy lime micrite	-	-0.62	-8.31	-	-	-	-	-	-	-	-	-
F1173	13.0	13.0	dgy lime micrite	-	-0.57	-9.16	-	-	-	-	-	-	-	-	-
F1173	13.5	13.5	dgy lime micrite	-	-0.28	-8.81	-	-	-	-	-	-	-	-	-
F1173	14.0	14.0	dgy lime micrite	-	-0.33	-7.93	0.70676	-	-	3512	1220	0.347	100.0	-	0.02686
F1173	14.5	14.5	dgy lime micrite	-	-0.16	-8.78	0.70679	-	-	2240	733	0.327	100.0	-	0.03638
F1173	15.0	15.0	dgy lime micrite	-	-0.26	-8.46	-	-	-	-	-	-	-	-	-
F1173	15.5	15.5	dgy lime micrite	-	-0.18	-9.03	-	-	-	-	-	-	-	-	-
F1173	16.0	16.0	dgy lime micrite	-	-0.77	-9.00	-	-	-	-	-	-	-	-	-
F1173	16.5	16.5	dgy lime micrite	-	-0.22	-9.21	0.70681	-	-	3084	663	0.206	95.9	-	0.03936
F1173	17.0	17.0	dgy lime micrite	-	-0.36	-8.50	0.70692	-	-	2924	905	0.297	96.0	-	0.10666
F1173	17.5	17.5	dgy lime micrite	-	-0.24	-6.51	0.70677	-	-	3340	1319	0.387	98.0	-	0.02427
F1173	18.0	18.0	dgy lime micrite	-	-0.38	-7.56	-	-	-	-	-	-	-	-	-
F1173	18.5	18.5	dgy lime micrite	-	-0.20	-9.15	-	-	-	-	-	-	-	-	-
F1173	19.0	19.0	dgy lime micrite	-	0.04	-9.02	0.70679	-	-	2372	509	0.202	94.1	-	0.03203
F1173	19.5	19.5	dgy lime micrite	-	0.04	-9.25	0.70683	-	-	2594	615	0.223	94.1	-	0.03571

F1173	20.0	20.0	dgy lime micrite	-	-0.09	-8.53	-	-	-					-	-
F1173	20.5	20.5	dgy lime micrite	-	-0.11	-9.23	0.70684	-	-	3240	662	0.200	98.0	-	0.02726
F1173	21.0	21.0	dgy lime micrite	-	-0.15	-9.81	0.70692	-	-	2062	538	0.250	96.0	-	0.02899
F1173	21.5	21.5	dgy lime micrite	-	-0.24	-8.66	-	-	-					-	-
F1173	22.0	22.0	dgy lime micrite	-	-0.03	-8.92	0.70686	-	-	2671	735	0.243	88.2	-	0.06239
F1173	22.5	22.5	dgy lime micrite	-	0.01	-9.01	-	-	-	-	-	-	-	-	-
F1173	23.0	23.0	dgy lime micrite	-	-0.60	-9.10	0.70681	-	-	3470	593	0.161	94.1	-	0.05661
F1173	23.5	23.5	dgy lime micrite	-	-1.50	-10.48	-	-	-	-	-	-	-	-	-
F1173	24.5	24.5	dgy lime micrite	-	-0.01	-8.79	-	-	-	-	-	-	-	-	-
F1173	25.0	25.0	dgy lime micrite	-	0.25	-8.62	-	-	-	-	-	-	-	-	-
F1173	25.5	25.5	dgy lime micrite	-	0.38	-9.14	0.70683	-	-	2675	381	0.140	98.0	-	0.03017
F1173	26.0	26.0	dgy lime micrite	-	0.34	-9.20	-	-	-	-	-	-	-	-	-
F1173	26.5	26.5	dgy lime micrite	-	0.09	-9.17	-	-	-	-	-	-	-	-	-
F1173	27.0	27.0	dgy lime micrite	-	0.73	-5.28	0.70684	-	-	1513	703	0.446	96.1	-	0.09318
F1173	27.5	27.5	dgy lime micrite	-	-0.68	-8.46	0.70687	-	-	2898	455	0.154	98.0	-	0.11465
F1173	28.0	28.0	dgy lime micrite	-	-0.23	-8.73	0.70701	-	-	2283	483	0.181	85.7	-	0.14863
F1173	28.5	28.5	dgy lime micrite	-	0.29	-7.65	-	-	-	-	-	-	-	-	-
F1173	29.5	29.5	dgy lime micrite	-	-0.02	-9.85	0.70692	-	-	2454	300	0.103	84.0	-	0.04424
F1173	30.0	30.0	dgy lime micrite	-	0.67	-9.90	-	-	-	-	-	-	-	-	-

(d)gy = (dark)grey, gs = grainstone, wacke = wackestone, ev = evaporite, wht = white, brecc = brecciated, dol = dolomite

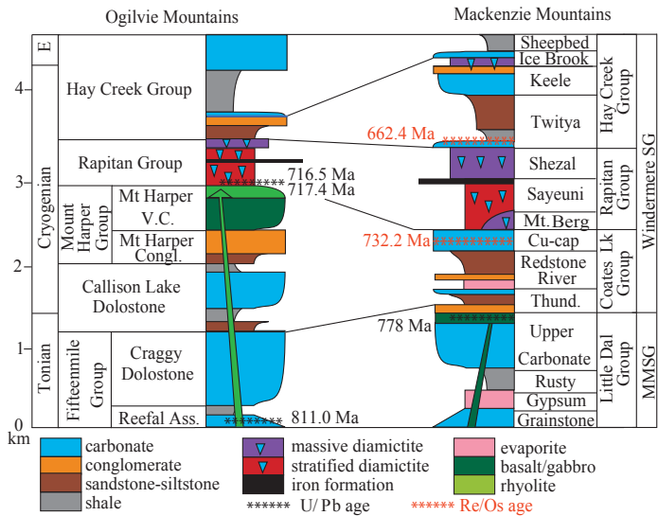
Ogilvie Mountains
Mackenzie Mountains
E
Cryogenian
Tonian
Hay Creek Group
Rapitan Group
Mount Harper Group
Mt Harper V.C.
Mt Harper Congl.
Callison Lake Dolostone
Fifteenmile Group
Craggy Dolostone
Reefal Ass.
716.5 Ma
717.4 Ma
811.0 Ma
662.4 Ma
732.2 Ma
778 Ma
Sheepbed
Ice Brook
Keele
Twitya
Shezal
Sayeuni
Mt. Berg
Cu-cap
Redstone River
Thund.
Upper Carbonate
Rusty
Gypsum
Grainstone
Hay Creek Group
Rapitan Group
Coates Lk Group
Little Dal Group
Windermere SG
MMSG
4
3
2
1
0
km
carbonate
conglomerate
sandstone-siltstone
shale
massive diamictite
stratified diamictite
iron formation
U/ Pb age
evaporite
basalt/gabbro
rhyolite
Re/Os age

Figure 1

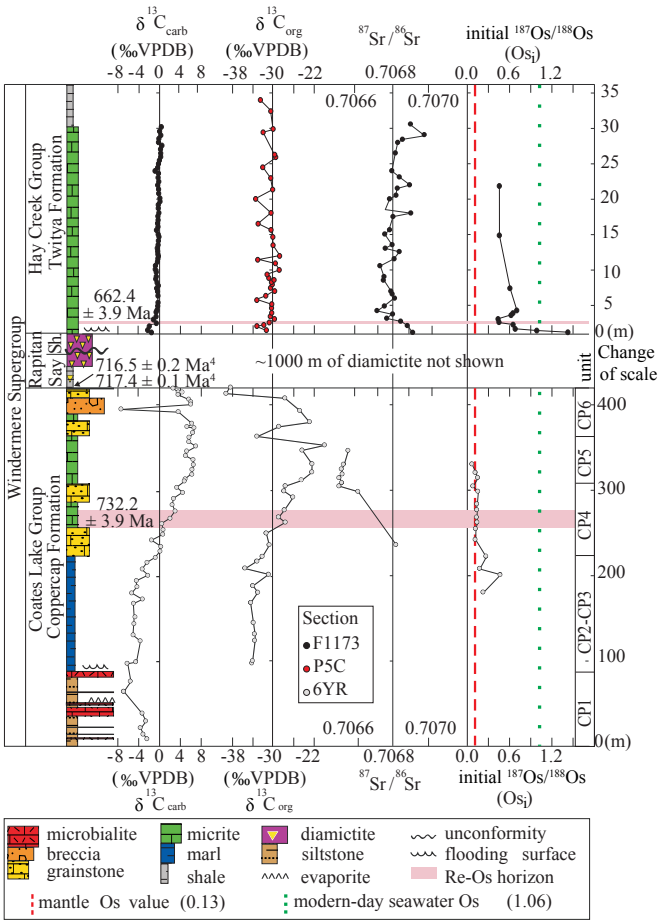
δ 13C carb (‰VPDB)
δ 13C org (‰VPDB)
87Sr/86Sr
initial 187Os/188Os (Osi)
-8 -4 0 4 8
-38 -30 -22
0.7068
0.0 0.6 1.2
0.7066
0.7070
35
30
25
20
15
10
5
0 (m)
Hay Creek Group
Twitya Formation
662.4 ± 3.9 Ma
Rapitan
Sayunei Fm
716.5 ± 0.2 Ma[4]
717.4 ± 0.1 Ma[4]
~1000 m of diamictite not shown
Change of scale unit
Windermere Supergroup
Coates Lake Group
Coppercap Formation
732.2 ± 3.9 Ma
400
300
200
100
0(m)
CP6
CP5
CP4
CP2-CP3
CP1
Section
F1173
P5C
6YR
microbialite
breccia
grainstone
micrite
marl
shale
diamictite
siltstone
evaporite
unconformity
flooding surface
Re-Os horizon
mantle Os value (0.13)
modern-day seawater Os (1.06)

Figure 2

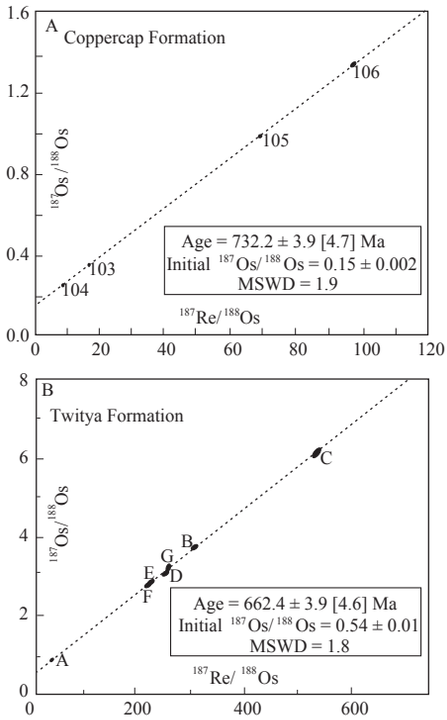
A
Coppercap Formation
106
105
103
104
Age = 732.2 ± 3.9 [4.7] Ma
Initial 187Os/188Os = 0.15 ± 0.002
MSWD = 1.9
187Os/188Os
187Re/188Os
1.6
1.2
0.8
0.4
0.0
0
20
40
60
80
100
120

B
Twitya Formation
C
B
G
E
D
F
A
Age = 662.4 ± 3.9 [4.6] Ma
Initial 187Os/188Os = 0.54 ± 0.01
MSWD = 1.8
187Os/188Os
187Re/188Os
8
6
4
2
0
0
200
400
600

Figure 3

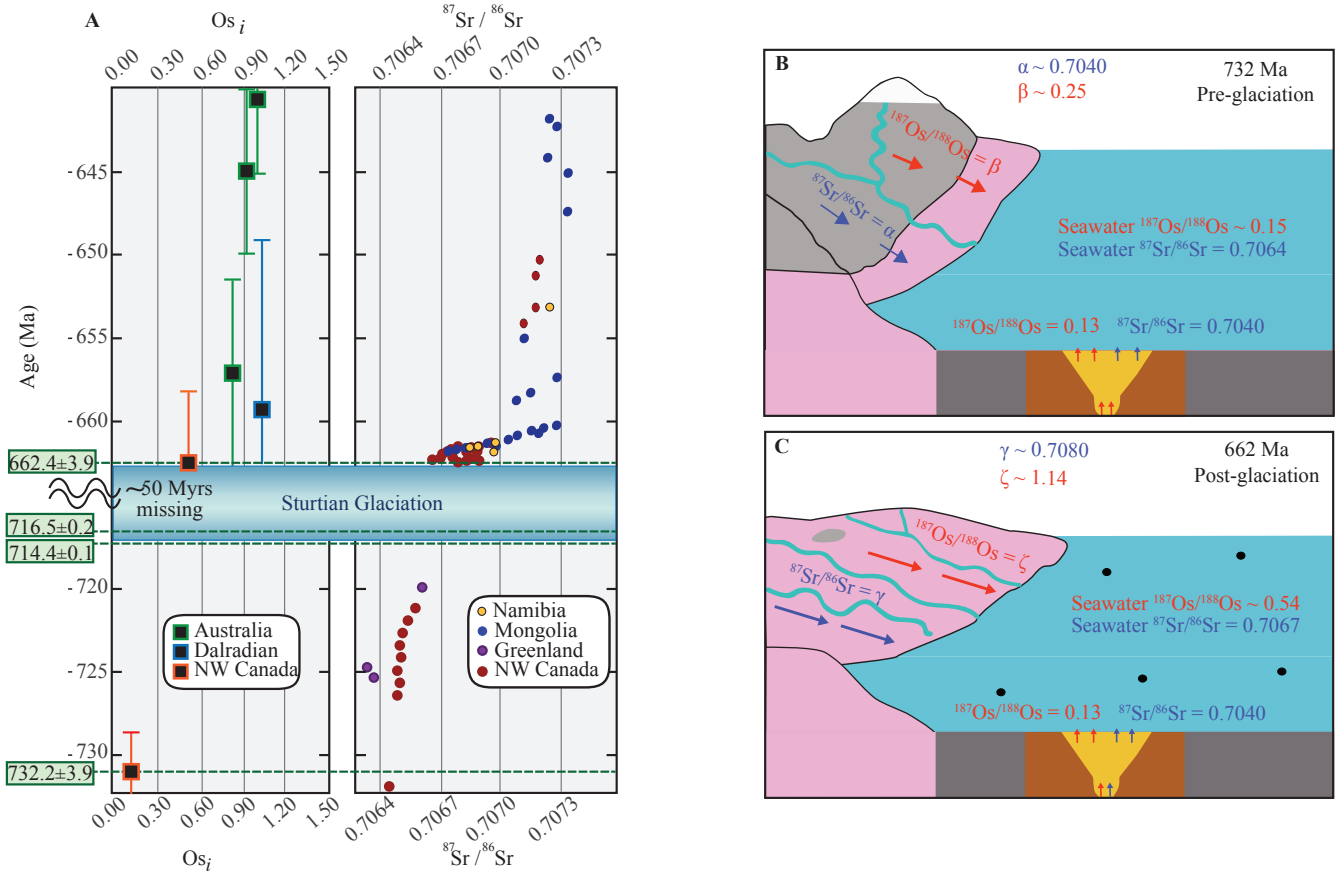
A
Os i
87Sr / 86Sr
0.00
0.30
0.60
0.90
1.20
1.50
0.7064
0.7067
0.7070
0.7073
Age (Ma)
645
650
655
660
662.4±3.9
~50 Myrs missing
Sturtian Glaciation
716.5±0.2
714.4±0.1
720
725
730
732.2±3.9
Australia
Dalradian
NW Canada
Namibia
Mongolia
Greenland
NW Canada
Osi
87Sr / 86Sr
B
α ~ 0.7040
β ~ 0.25
732 Ma
Pre-glaciation
187Os/188Os = β
87Sr/86Sr = α
Seawater 187Os/188Os ~ 0.15
Seawater 87Sr/86Sr = 0.7064
187Os/188Os = 0.13
87Sr/86Sr = 0.7040
C
γ ~ 0.7080
ζ ~ 1.14
662 Ma
Post-glaciation
187Os/188Os = ζ
87Sr/86Sr = γ
Seawater 187Os/188Os ~ 0.54
Seawater 87Sr/86Sr = 0.7067
187Os/188Os = 0.13
87Sr/86Sr = 0.7040

Figure 4

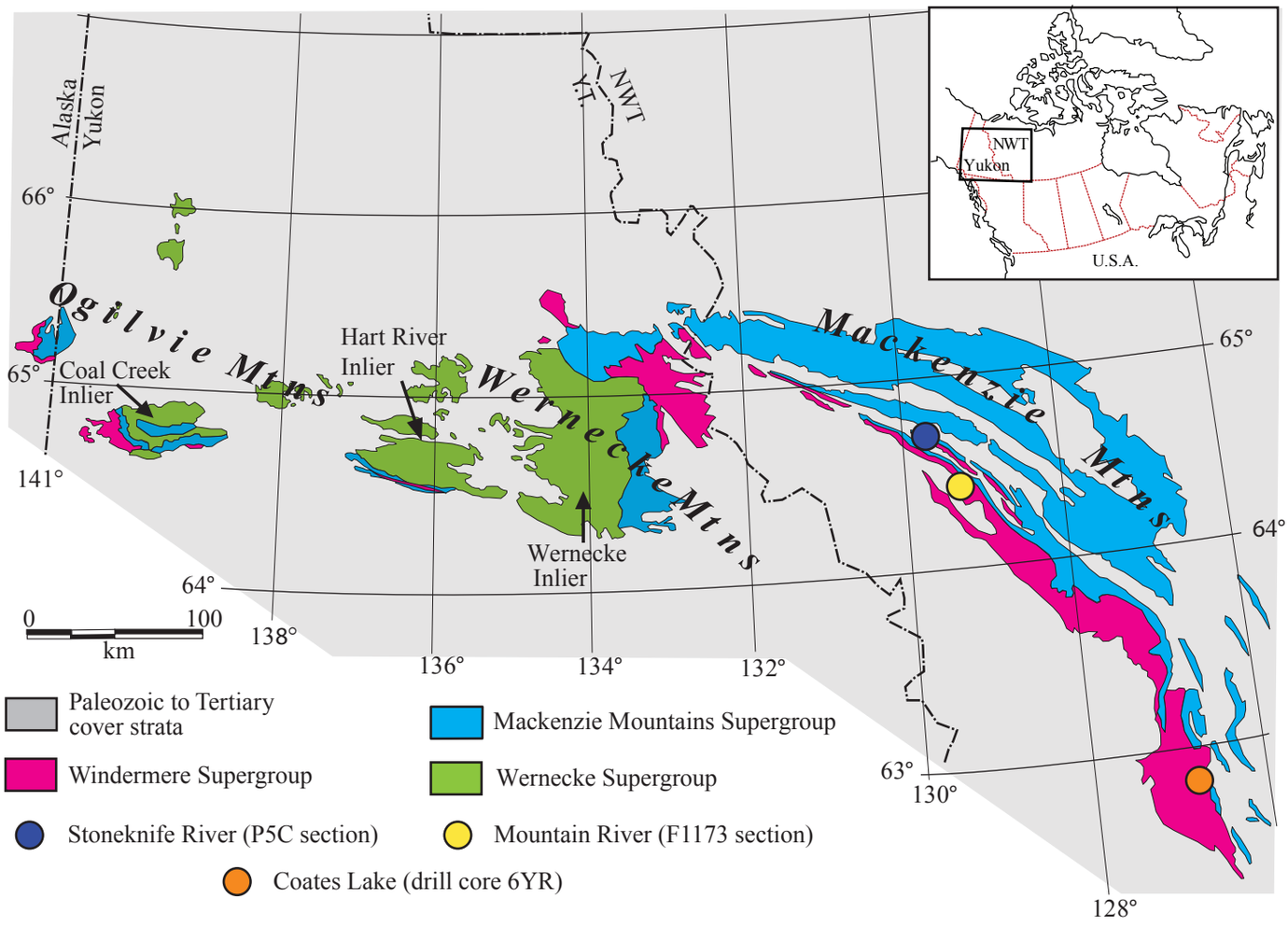
Alaska
Yukon
NWT
66°
65°
141°
Ogilvie Mtns
Coal Creek
Inlier
Hart River
Inlier
Wernecke Mtns
Wernecke
Inlier
Mackenzie Mtns
65°
64°
64°
0
100
km
138°
136°
134°
132°
130°
63°
128°
NWT
Yukon
U.S.A.
Paleozoic to Tertiary
cover strata
Mackenzie Mountains Supergroup
Windermere Supergroup
Wernecke Supergroup
Stoneknife River (P5C section)
Mountain River (F1173 section)
Coates Lake (drill core 6YR)

Figure S1

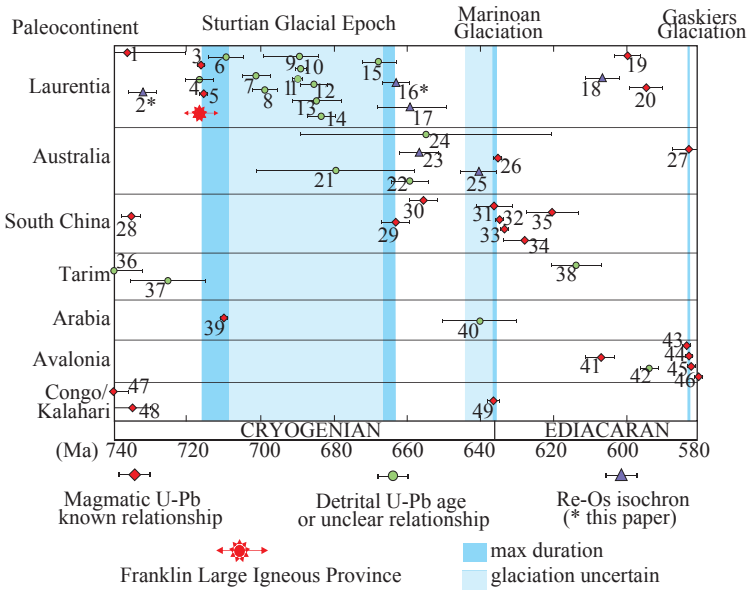
Paleocontinent
Sturtian Glacial Epoch
Marinoan Glaciation
Gaskiers Glaciation
Laurentia
Australia
South China
Tarim
Arabia
Avalonia
Congo/ Kalahari
CRYOGENIAN
EDIACARAN
(Ma) 740 720 700 680 660 640 620 600 580
Magmatic U-Pb known relationship
Detrital U-Pb age or unclear relationship
Re-Os isochron (* this paper)
Franklin Large Igneous Province
max duration
glaciation uncertain

Figure S2